A High Speed Functional MicroCT Detector For Small Animal Studies

Vivek V. Nagarkar[1], Sameer V. Tipnis[1*], Irina Shestakova[1],Valeriy Gaysinskiy[1], Bipin Singh[1], Michael J. Paulus[2], Gerald Entine[1]

Abstract-- **Dedicated MicroCT systems for noninvasive screening of small animals are now in routine use. However, speed of operation limits their use for functional studies. At RMD we are addressing this need by developing a digital x-ray detector that can simultaneously provide high speed, high sensitivity, and a large active imaging area. The system consists of a special high speed CCD detector optically coupled to a scintillator. In its current configuration, the system provides 5 x 5 cm^2 active area, spatial resolution of ~100 μm, and can operate at speeds of up to 225 frames per second. The system has been used to acquire volumetric CT data with 360 projections in ~12 seconds compared to several minutes needed for most commercial systems. This paper presents design of various system components and performance characterization along with the CT reconstruction data on a mouse phantom.**

I. Introduction

Dedicated high-resolution small animal imaging systems have recently emerged as important new tools for cancer research [1,2,3,4]. These systems permit noninvasive screening of animals for mutations or pathologies and to monitor disease progression and response to therapy. Among these, x-ray microcomputed tomography (microCT), shows promise as cost-effective means for detecting and characterizing soft tissue structures, skeletal abnormalities, and tumors in live animals [5]. Current CT systems provide high-resolution images with excellent sensitivity to skeletal tissue and good sensitivity to soft tissue, particularly when contrast-enhancing media are employed. However, use of this powerful modality for functional studies such as those of tumor vascular physiology or involving true whole organ physiologic imaging is difficult due to the lack of a suitable x-ray imaging detector. Typically, such studies require a detector that can simultaneously provide high speed, high sensitivity, and a large active imaging area.

At RMD we are developing a high-speed, high-sensitivity, large area x-ray detector to address these needs. The detector is based on a new electron multiplying CCD (EMCCD) coupled to a high sensitivity, high-resolution microcolumnar CsI(Tl) scintillator via a fast lens. This new CCD not only provides high resolution and low noise, but also internal avalanche gain. The presence of an internal gain effectively reduces the read noise even when operated at high frame rates of 225 fps, thus improving the image SNR. This feature allows construction of a high speed tomographic imaging system than can be used for functional imaging in small animals. Here we discuss the system design including the choice of scintillator for high-speed imaging and preliminary performance characterization of the small animal CT system based on these components.

II. Scintillators For High Speed Imaging

Scintillators for high-speed x-ray imaging

High-speed imaging applications are inherently light-starved. The problem is made worse when the source of light is the passive output of an x-ray scintillator screen. Thus, in such applications a premium is placed on the x-ray to light conversion efficiency of the screen. Additionally, the speed of emission or fast decay time is critical to ensure minimized blurring due to persistence. Also, high x-ray stopping power is necessary to maximize the x-ray absorption and thus minimizing noise. We have identified several candidate scintillators that satisfy these criteria. Table 1 lists these candidate materials and their scintillation properties. Although GOS(Tb) is known to have a long decay time, it was included in the evaluation as a reference screen since this screen is currently employed in existing CCD-based CT detectors.

Scintillator screens of all the materials outlined in Table 1, except the CsI(Tl), are powdered screens. Both, GOS(Pr) and GOS(Tb) are commercial screens, whereas the screens of other materials were specially developed during this study. The CsI(Tl) material was vapor deposited on fiberoptic and

Manuscript received October 18, 2004. This work was supported in part by NIH Grant # 03-220-3110.

V. V. Nagarkar is with Radiation Monitoring Devices (RMD), Inc., Watertown, MA 02472 USA (telephone: 617-668-6937, e-mail: vnagarkar@ rmdinc.com).

S. Tipnis was with Radiation Monitoring Devices (RMD), Inc. He is now with Department of Radiology, West-2, Mayo Clinic, 200 First Street SW, Rochester, MN 55905, USA (e-mail: Tipnis.Sameer@mayo.edu)

I. Shestakova is with Radiation Monitoring Devices (RMD), Inc., Watertown, MA 02472 USA (telephone: 617-668-6933, e-mail: ishestakova@ rmdinc.com).

V. Gaysinskiy is with Radiation Monitoring Devices (RMD), Inc., Watertown, MA 02472 USA (telephone: 617-668-6931), e-mail: vgaysinskiy@ rmdinc.com).

B. Singh is with Radiation Monitoring Devices (RMD), Inc., Watertown, MA 02472 USA (telephone: 617-668-6934), e-mail: bsingh@ rmdinc.com).

M. J. Paulus is with Imtec, Inc., Knoxville, TN, USA (telephone: 865 521-7025, e-mail: paulusmj@imtekinc.com).

Gerald Entine is with Radiation Monitoring Devices (RMD), Inc., Watertown, MA 02472 USA (telephone: 617-668-6806), e-mail: gentine@ rmdinc.com).

Scintillator Material	Screen Form	Decay Time (ns)	Afterglow	Conversion Efficiency (Ph/MeV)	Wavelength of Peak Emission (nm)	CCD QE (%) Front Ill.	Material Density (g/cc)
CsI(Tl)	Columnar	680	Yes	61,000	540	35	4.51
Gd_2O_2S(Pr) or GOS(Pr)	Powder	2700	No	30,000	540	35	7.8*
$Y_3Al_5O_{12}$(Ce) or YAG	Powder	88	No	19,700	550	35	4.55*
$CaWO_4$	Powder	6,000	No	18,000	470	15	6.1*
Gd_2O_2S(Tb) or GOS(Tb)	Powder	>1 ms	No	30,000	540	35	7.8*

Table 1. Properties of scintillators important for high-speed imaging

*The screen density is approximately 60% of the material density.

graphite substrates to form a high resolution microcolumnar screen using the technology previously developed at RMD.

Scintillation decay characterization

For scintillation decay characterization screens were excited with 20 ns (FWHM), 300 kVp x-ray pulses using model XRS-3 x-ray generator from Golden Engineering, Inc. The scintillation light from the screens was passed through a model 234/302-0.2m McPherson monochromator, detected by a Hamamatsu R2059 photomultiplier (PMT), and recorded by a Tektronix TDS220 digital storage oscilloscope. In this specially developed setup, both time and signal domains span nine orders of magnitude.

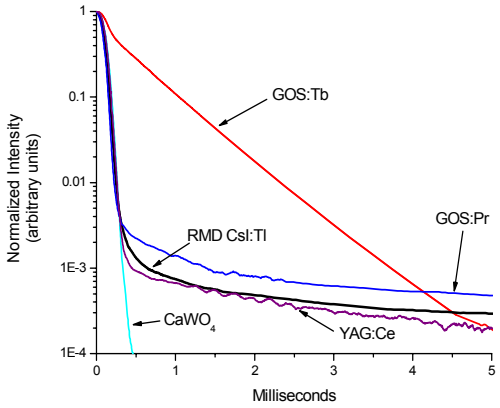

Figure 1. Decay characteristics of various screens. All the screens are fast enough for targeted 300 fps imaging, except GOS(Tb) which may show some image blurring at high frame rates.

Figure 1 shows decay time characteristics of various screens under evaluation. As can be seen from the figure, screens made from CsI(Tl), GOS(Pr), YAG, and $CaWO_4$ show a very rapid decay (τ = 1/e) of few microseconds or less, except for GOS(Tb) which decays in approximately 1 ms. Also, most of these screens show finite residual intensity even up to 5ms after excitation due to their known afterglow characteristics. However, the residual intensity is small enough ($<10^{-3}$ of initial intensity) so that these screens can be used for 300 fps (3.3 ms/frame) imaging which is of interest in this application. Although GOS(Tb) exhibit a slow decay, it does not have any appreciable afterglow after 5 ms, and it decays to a 0.001% intensity level in 3.5 ms. Thus, all the screens tested are fast enough for our targeted imaging speed of 300 fps and the ultimate choice of the suitable scintillator was determined by other properties such as light output efficiency, spatial resolution and noise.

III. Imaging Performance

Experimental Setup

For these measurements the scintillator films were coupled to a 1024 × 1024 pixel thermoelectrically cooled CCD optically bonded to a 3:1 fiberoptic taper. The CCD pixel size is 19 µm and with the fiberoptic taper the effective pixel size is 57 µm resulting in a Nyquist limiting frequency of 8.6 lp/mm. The CCD device, the readout electronics (including a 12 bit ADC)[9] and the image processing software operate on a PC platform. The x-ray source used for these measurements was a Gendex Series 1000, tungsten target, 40-110 kVp continuously variable energy source. For the measurements reported here, it was set to 40 kVp. The source-to-detector distance was maintained at 65cm.

Light output measurements

Light output measurements were made by exposing the detector to a uniform flood field of x-rays, and averaging analog to digital unit value (ADUs) in a pre-defined region of interest (ROI). For each measurement the x-ray exposure was estimated using an air ionization chamber (Nuclear Associates Model 06-526-5280). Several measurements per screen were made to improve the statistical accuracy of the ADU value. These data were corrected for any variations in the measured x-ray exposure. The signal to noise ratio (SNR) in each screen was computed by dividing the average ADU value by the measured standard deviation in the flood image. Resulting data are shown in Figure 2.

CsI(Tl) screen exhibited excellent light output, even though it is significantly thinner than GOS(Tb). This was attributed primarily to the high scintillation light yield of CsI(Tl), which significantly improves SNR. This is evident from the SNR for CsI(Tl) which was the highest measured as seen in Figure 2.

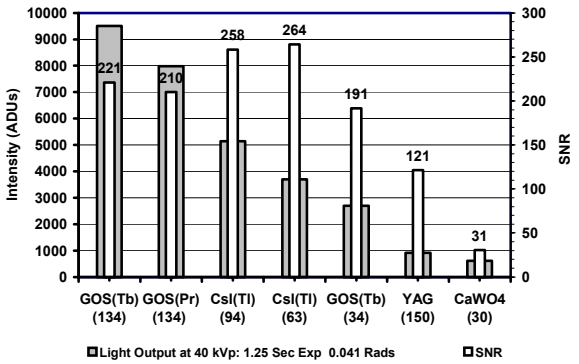

Figure 2. Light output and SNR and of various scintillator screens. The numbers in parentheses are the screen thicknesses in terms of mg/cm^2.

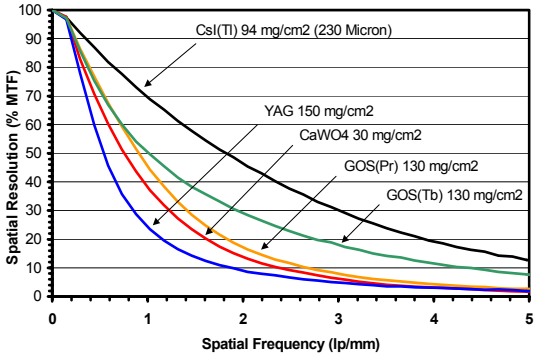

Figure 3. Spatial resolution of various screens under evaluation

Spatial Resolution Measurements

To evaluate spatial resolution of screens, the pre-sampling MTF was measured according to the technique described by Fujita et al [6] and others [7,8,9]. An image of a long, 10-µm (±1 µm) wide slit made of 1.5 mm thick tantalum placed at a slight angle (less than 4 degrees) to the pixel matrix at the center of the detector was obtained. The area around the slit was covered with 0.5 cm thick lead. The slit was placed in contact with the surface of the imager so that the spreading of the Line Spread Function (LSF) due to the finite size of the focal spot did not pose a significant limitation. The exposure was adjusted by varying the mAs while maintaining a constant 40-kVp, to ensure that the tails of the LSF had no significant electronic noise. The finely sampled LSF was normalized to a peak value of one. The Fourier Transform (FT) of the finely sampled LSF was performed to provide the presampling MTF. shows the measured MTF as a function of spatial frequency.

As expected microcolumnar CsI(Tl) screens show substantially higher MTF compared to the other screens of comparable thickness. Specifically, 230 µm thick screen (94 mg/cm^2) shows resolution of >5 lp/mm. When combined with its high light output, low noise, and excellent speed of response, CsI(Tl) appears to be the best choice for the present application. Also, the GOS(Pr) screen shows a good resolution of 3 lp/mm. Although the resolution is not as high as the CsI(Tl), with its high light output, rapid decay, and absence of substantial afterglow, GOS(Pr) screens may also be a good choice for some applications.

IV. EMCCD READOUT

Electron multiplying CCD works like a conventional CCD, except that it provides an internal gain via an avalanche mechanism. As such, an imaging system based on the EMCCD does not require the use of intensification stages even though it provides detection of extremely low light levels. An important advantage of EMCCD is that it effectively reduces the read noise by the gain factor, thereby improving the output SNR, even under conditions of very high frame readouts of 300 fps. As usual, cooling the chip can control the dark noise. Thus, with its very low total noise(<1 e-), cooled EMCCDs are ideally suited for high speed imaging operation.

In the present work we have used commercially available EMCCD model Cascade 512F camera from Roper Scientific, NJ [10]. This CCD is based on an E2V CCD87 chip, and its specifications are summarized in Table 2**.** In this system, the serial readout is performed at a rate of 10 million pixels per second, thus the entire 512 x 512 pixel data is read out in ~26 ms or a maximum speed of ~30 frames per second. Higher frame rates of 300 fps and above can be achieved by sacrificing the pixel resolution as shown in Table 3. We have used this feature to image up to 512 x 64 pixels at the frame rates of ~240 fps.

Parameter	**Specification**
CCD Chip	E2V CCD87
CCD Format	512 x 512 Pixels
Pixel Size	16 µm Square
Full well capacity	250 ke-
Gain register capacity	850 ke-
Readout	16 bits; 10MHz
On-chip gain	1 to >1000x
Operating temperature	-30C
Dark current	1 e-/pixel/sec @-30C
Binning	Flexible binning

Table 2. Cascade 512F Camera Specifications

Pixel Resolution	**Measured Frame Rate (Frames / second)**
512 x 512	30
512 x 256	60
512 x 128	120
512 x 64	240
512 x 32	480

Table 3. Measured frame rates for the Cascade 512F camera as a function of pixel resolution.

V. Detector Design

The detector consisted of the lens based EMCCD camera attached to a specially designed light tight box. The front end of the box was covered with a low x-ray absorption Be window. A sliding assembly was incorporated in the box to mount 10 x 10 cm area scintillator and to adjust its position relative to the CCD. A fast lens (f/0.95) was used to directly image the scintillator screen onto the CCD chip. To ensure high sensitivity and low noise, the CCD gain was set at ~50 which provided maximum dynamic range of 14 bits.

High Speed Radiographic X-ray Imaging

To test the dynamic x-ray imaging capability of the system, a mechanical, steel toy consisting of several wheels was used as test object. The toy could be "wound up" and on release, the various wheels would move at varying speeds of 60 to 120 rpm, providing a dynamically moving test object. This toy (Figure 4(a)) was imaged using 120 kVp x-rays from an Electromed CPX 160 model tungsten target, 60 KW x-ray generator , set at 50 mA and running in continuous mode. The camera gain was set at 40. Dynamic x-ray images of the moving parts of the toy acquired with a 230 µm thick CsI(Tl) screen at speeds of 30, 50, 90, 120 and 225 fps and are shown in Figure 4(b-f). As pointed out before, with increasing frame-rates (speeds), the effective imaging area of the camera is reduced in the vertical dimension. As can be seen from the figures, motion blur arising from the high speed rotation of the gears is significantly reduced as the imaging speed is increased.

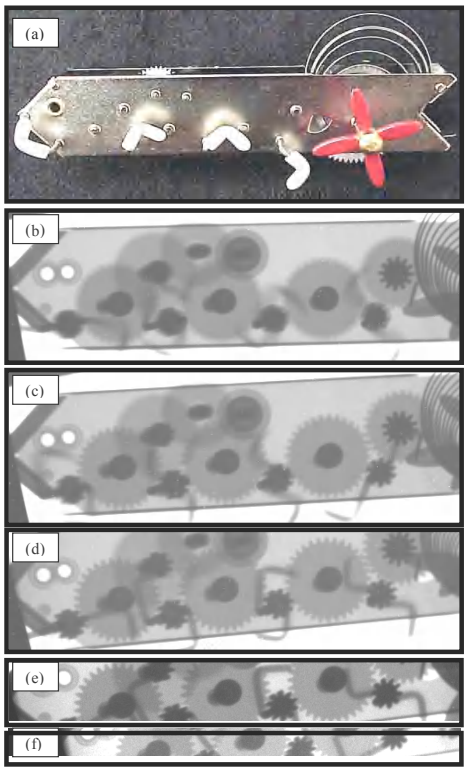

Figure 4. Dynamic images (unprocessed) of a toy (a) the toy, (b) at 30 fps, (c) at 50 fps, (d) at 90 fps, (e) 120 fps, and (f) at 225 fps. The gears are made from plastic and metal, and depending on their diameter are moving at a speed of up to 120 rpm.

VI. High Speed CT

Experimental Setup

The experimental setup for acquiring CT data is shown in Figure 5. The source to detector distance was 12.2 cm and the source to object distance was 9.5 cm. This resulted in the image magnification of 1.28. A digitally controlled stage was used to rotate the test phantom to obtain 360° projection data. This stage offered a maximum speed of 29°positions/second or ~12.4 seconds for a full rotation. The x-ray source used was a SRI, Inc. Model SB-80-500, 40Watt, tungsten anode x-ray generator with a 50 µm focal spot [11]. The output range on this source is 30-80 kVp, 5-500 µA max.

A 'mouse' phantom consisting of a ~ 2.5 cm diameter, 5 cm long Lucite cylinder with two ~ 1 cm diameter holes representing mouse lungs, and a 3 mm diameter hole fitted with a bone equivalent material representing the mouse spine. The Lucite itself is considered to be tissue equivalent material. Figure 6(a) shows the photograph of the mouse phantom.

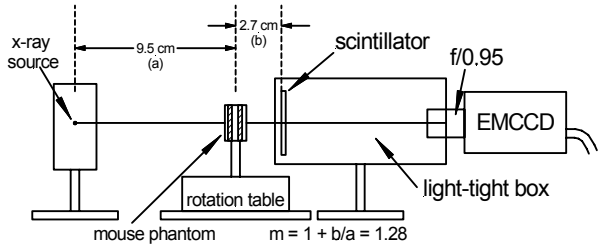

Figure 5. Schematic of the proposed Phase II high speed CT scanner based on a novel x-ray detector. The new design of this detector will allow imaging at the speed of up to 300 fps and will permit acquisition of full volumetric data in seconds.

High Speed CT of a Mouse Phantom

For these experiments, the source was operated at 64 kVp, 400 µA, or ~25 Watts. A 1 mm thick Al was used to filter the low energy x-ray component form the emerging beam. The estimated x-ray dose for the entire 360° scan was ~5 cGy. Cone beam CT data on a mouse phantom were acquired at various frame rates ranging from 30 fps to 120 fps using a 230 µm thick CsI(Tl) scintillator screen. The entire 360° projections data set was acquired in 12.4 seconds, corresponding to the fastest allowed speed of the rotation stage. A set of 100 dark and 100 flood images were acquired for flat-field correction at each speed.

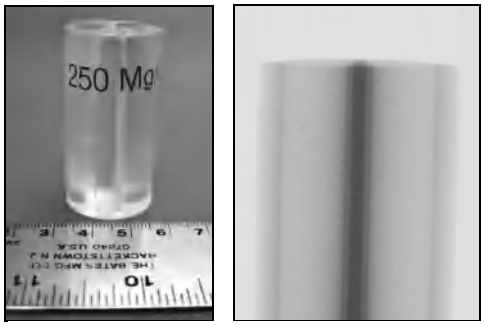

(a) (b)

Figure 6. (a) Photograph of the mouse phantom**. (b)** Image of the phantom acquired at 30 fps using EMCCD based detector.

During data acquisition the object was continuously irradiated throughout the length of the scan without the use of a shutter. This did not produce any appreciable image blur due to the very high rate of 'on-chip' data transfer offered by the EMCCD architecture.

The image data were reconstructed using the Feldkamp reconstruction algorithm. No corrections were introduced for lens distortion or bad CCD pixels. Projection images show some "hot" image pixels generated by direct interaction of the x-ray photons in the CCD. No corrections were introduced for these hot pixels and the dark streak artifacts in the images are attributed to these "hot" pixels. A two dimensional cross-section and surface renderings of the data acquired at 30 fps are shown in Figure 7. Note that the presence of thin adhesive tape on the mouse phantom is clearly seen in the surface renderings indicating the resolution capability of the prototype CT system.

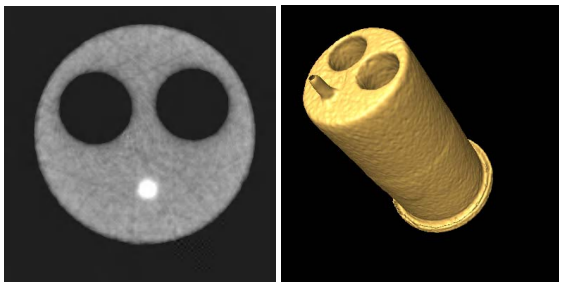

(a) (b)

Figure 7. A two dimensional cross section and surface renderings of the data acquired at 30 fps**.** Note that the presence of thin adhesive tape on the mouse phantom is clearly resolved in the surface renderings indicating the resolution capability of the detector.

These data illustrate an important aspect of the imaging system, namely, the high quality of images when operated in the high-speed mode, which is critical in functional imaging. This combined with the reduced dose should make such a system particularly useful for functional micro-CT.

VII. CONCLUSION

We have developed a prototype high-speed x-ray imaging system which was used to acquire projection images at the rate of up to 225 fps. Utility of this system for small animal CT was demonstrated by acquiring a full set of cone beam CT on the mouse phantom in 12.4 seconds, with a total exposure of only 5 cGy. The acquisition speed was limited only by the rotational speed of the object positioning unit. This is a significant accomplishment and represents over an order of magnitude increase in data acquisition speed compared to the current commercial systems. With such high-speed data acquisition, the CT system, can now be used for functional studies such as those of tumor vascular physiology or whole organ physiologic imaging. Work in this regard is currently underway at RMD. We are also focusing on improving the detector sensitivity through the use of a fiberoptic coupler and a back-thinned version of the EMCCD. Also, we are developing a new x-ray generator that can simultaneously provide high power, small focal spot, and kVp settings in the range of 20 to 70 kVp, required for high-resolution small animal imaging at high speeds without being limited by the x-ray fluence.

V. ACKNOWLEDGEMENT

This work was supported in part by NIH grant # 1 R43 CA01871-01.

VI. REFERENCES

[1] Hounsfield GN (1973). Computerized transverse axial scanning (tomography): 1. Description of system. *BrJ Radial* 46,1016-. 1022.

[2] Lauterbur PC (1973). Image formation by induced local interactions — examples employing nuclear magnetic resonance. *Nature* **242,**

[3] Tar- Pogossian MM, Phelps ME, and Mullanl NA (1975). A positron-emission transaxial tomography for nuclear imaging (PETT). *Radiology* 114, 89—98.

[4] Kuhl DE, and Edwards HO (1963). *Radiology* 80, 653—662.

[5] Paulus MJ, Sari - Sarraf H, Gleason 85, Bobrek M, Hicks JS, Johnson OK, Behel JK, Thompson LH, and Allen WC (1999). A new X-ray computed tomography system for laboratory mouse imaging. *IEEE Trans Nucl Sd* ***46,*** 558—564.

[6] Fujita, H., D.Y. Tsai, T. Itoh, K. Doi, J. Morishita, K. Ueda and A. Ohtsuka. (1992). "A simple method for determining the modulation transfer function in digital radiography." *IEEE Trans. Med. Imaging* MI-11: 34-39

[7] Vedantham, S., A. Karellas, S. Suryanarayanan, D. Albagli, S. Han, E. Tkaczyk, C. Landberg, B. Opsahl-Ong, P. Granfors, I. Levis, C.J. D'Orsi and R.E. Hendrick. (2000). "Full Breast Digital Mammographic Imaging with an Amorphous Silicon-based Flat Panel Detector: Physical Characteristics of a Clinical Prototype." *Med. Phys.* 27: 558-567.

[8] Vedantham, S., A. Karellas, S. Suryanarayanan, M. Sayag, R. Kleehammer, R. Heidsieck and C.J. D'Orsi. (2000). "Mammographic imaging with a small format CCD-based digital cassette: Physical characteristics of a clinical system." *Med. Phys.* 27(8): 1832-1840.

[9] Dobbins, J.T., D.L. Ergun, L. Rutz, D.A. Hinshaw, H. Blume and D.C. Clark. (1995). "DQE(f) of four generations of computed tomography acquisition devices." *Med. Phys*. 22(10): 1581-1593.

[10] http://www.photomet.com/pdfs/datasheets/cascade/512F.pdf

[11] SourceBlock Product Family, SB-80-500, Source-Ray, Inc., 167 Keyland ct., Bohemia, NY 11716, phone (631)-244-8200.